

Dissociation of Eu^{+3} Charge-Transfer State in $\text{Y}_2\text{O}_2\text{S}$ and $\text{La}_2\text{O}_2\text{S}$ into Eu^{+2} and a Free Hole

C. W. Struck and W. H. Fonger
RCA Laboratories, Princeton, New Jersey 08540
 (Received 1 March 1971)

In $\text{Y}_2\text{O}_2\text{S}:\text{Eu}$ and $\text{La}_2\text{O}_2\text{S}:\text{Eu}$, excitation into the charge-transfer states (CTS) of Eu^{+3} leads partially to the dissociation of the CTS into Eu^{+2} and a free hole which may subsequently be trapped. The extent of CTS dissociation is measured both by the storage induced by a known CTS excitation dosage and by the slow-rise transients of the 5D emissions at the onset of CTS excitation. Both measurements give an activation energy for CTS dissociation of 900 cm^{-1} for $\text{Y}_2\text{O}_2\text{S}$ and 1300 cm^{-1} for $\text{La}_2\text{O}_2\text{S}$, and a rate constant of $\sim 10^{13.5}\text{ sec}^{-1}$ for both hosts. The steady-state emission intensity undergoes a gradual superlinear transition with excitation intensity. The time constant of the slow-rise transient decreases with excitation intensity. The phosphorescence intensity is smaller than that of the slow-rise transient and increases sublinearly with excitation intensity. These kinds of behavior are all explained with the model of the CTS dissociating into Eu^{+2} and a free hole, with subsequent hole trapping and Eu^{+2} -trapped-hole nonradiative recombination. In this model, the Eu^{+2} concentration at steady state increases as the $\frac{1}{2}$ to $\frac{1}{3}$ power of the excitation intensity.

I. INTRODUCTION

A. Historical

In $\text{Y}_2\text{O}_2\text{S}:\text{Eu}$ and $\text{La}_2\text{O}_2\text{S}:\text{Eu}$, concentration- and temperature-dependent storage and loss occur¹ from the Eu^{+3} charge-transfer states (CTS) in competition with CTS \rightarrow 5D feeding. Excitation directly into the 5D states also leads at times to both storage¹⁻³ and loss,¹ but only if the 5D states are being thermally emptied to the CTS via 5D -CTS crossovers.^{4,5} The long times of the storage argue for some separation of charges. Forest, Cocco, and Hersh³ and we¹ both proposed that the Eu^{+3} CTS dissociates into Eu^{+2} and a free hole. Forest *et al.* also suggested the possibility that Eu^{+3} might ionize into Eu^{+4} and a free electron, but we regard this possibility as unlikely.

It was evident from our studies that losses and storage were intimately related, in that the excitation conditions which produced losses at high Eu concentration were the excitation conditions which produced storage at low Eu concentration. Thus, we proposed¹ that the losses similarly commence with the CTS dissociating into Eu^{+2} and a free hole but that, at high Eu concentration, the extra electron at the Eu^{+2} center can wander among the Eu sites, find a trapped hole, and combine nonradiatively with it. This paper reports further manifestations of energy loss and storage and further applications of the model of the CTS dissociating into Eu^{+2} and a free hole.

B. Synopsis of Effects to be Reported

In oxysulfide:Eu phosphors, the $^5D \rightarrow ^7F$ emission intensity in response to a long pulse of CTS excitation had the behavior shown in Fig. 1. The emission built up rapidly (in a few 5D lifetimes) to an initial

value B_0 and then slowly increased to a higher level B_∞ . When excitation was removed, the emissions fell rapidly to a level B_p and then slowly to zero. In Fig. 1, and in later figures showing detailed measurements, excitation G and emission intensity $B(t)$ are given in units such that B_∞/G is the steady-state quantum efficiency for all $^5D \rightarrow ^7F$ emissions.

The B_0/G depended upon sample history and was smallest when the phosphor had been previously exhausted of storage by heating or by infrared radiation (IR). This smallest B_0/G was independent of Eu concentration and of excitation intensity and decreased with increasing temperature from near unity at low temperature to about 0.1 at 500°K . At low temperatures B_∞/G was near unity. At high temperatures, particularly at high Eu concentration, B_∞/G increased with G —from near B_0/G at low G to near unity at high G .

The time constant of the slow rise from B_0 to B_∞ decreased sublinearly⁶ with excitation intensity G .

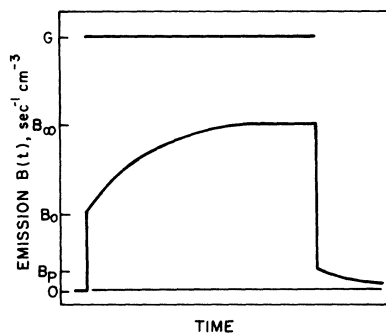


FIG. 1. Transient response of an oxysulfide:Eu phosphor to a long CTS excitation pulse of intensity G .

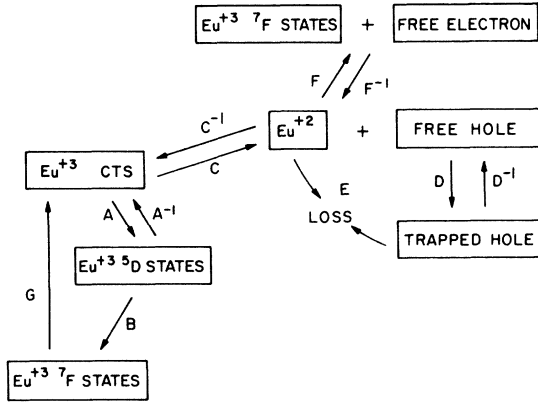


FIG. 2. Diagram of storage-loss processes in oxysulfide:Eu phosphors. Vertical displacement is a rough energy scale.

The B_p was asymmetric with the buildup in the sense that $B_p < B_\infty - B_0$, and B_p increased sublinearly with G .

These various kinds of behavior will be described in detail and accounted for with the model of the CTS dissociating into Eu^{+2} and a free hole.

II. MODEL

A. Diagram of Storage-Loss Mechanism

The storage and loss processes associated with dissociation of the CTS are diagrammed in Fig. 2. Process G is ${}^7F \rightarrow$ CTS excitation. Process A is CTS feeding of the 5D states; A^{-1} is inverse 5D thermal quenching to the CTS. Process B is $\text{Eu}^{+3} {}^5D \rightarrow {}^7F$ line emission. Process C is thermal dissociation of the CTS into Eu^{+2} and a free hole; C^{-1} is inverse formation of the CTS from Eu^{+2} and a free hole. Process D is trapping of free holes; D^{-1} is inverse freeing of trapped holes (either thermally or via IR stimulation). Process E is nonradiative recombination of Eu^{+2} and a trapped hole. Process F is dissociation of Eu^{+2} into Eu^{+3} and a free electron; F^{-1} is inverse formation of Eu^{+2} from Eu^{+3} and a free electron. Luminescence under band-gap excitation proceeds via the sequence F^{-1} , C^{-1} , A , B .

Following dissociation of the CTS, the free hole is quickly either trapped (D) or destroyed by recombining with an available Eu^{+2} (C^{-1}). The free-hole concentration is always relatively small, and the Eu^{+2} effective negative charge is balanced by the positive trapped-hole charge. Loss and storage are complementary processes. At high temperatures and high Eu concentrations, the extra electron forming the Eu^{+2} center is mobile among the Eu sites, can find a trapped hole, and can recombine with it nonradiatively at the trap site. At low temperatures and low Eu concentrations, the extra elec-

tron is bound tightly to its originating Eu site, and the Eu^{+2} and trapped-hole charges can remain stored. This storage can be retrieved as $\text{Eu}^{+3} {}^5D \rightarrow {}^7F$ line emissions if thermal or IR stimulation is provided which triggers the sequence D^{-1} , C^{-1} , A , B without triggering the process F .

When losses are important, the steady-state emission increases superlinearly with excitation intensity. The source of this nonlinearity is the change of the recombination route of the free holes with excitation intensity. At low intensity, most free holes are trapped and then recombine nonradiatively with Eu^{+2} at trap sites (sequence D , E). At high excitation intensity, more of the free holes find available Eu^{+2} s before they become trapped and produce additional emission via the sequence C^{-1} , A , B .

Formulas for the rates of the processes A through F^{-1} are given in Table I. The quantities used in these formulas are defined in Table II. The concentrations \bar{p}_0 , \bar{p}_i , and \bar{n}_0 are similar to barred concentrations used in the Hall-Shockley-Read theory of recombination^{7,8} in semiconductors.

B. Configurational-Coordinate Diagram Handling Capture and Release of Electrons and Holes

We have previously given a configurational-coordinate diagram which handled CTS $\rightarrow {}^5D$ feeding transitions and inverse ${}^5D \rightarrow$ CTS quenching transitions.^{4,5} The capture and release of electrons and holes at the Eu center can also be included in a configurational-coordinate diagram. This more complete diagram is given in Fig. 3. This figure differs from the earlier figure (Fig. 1 of Ref. 4) by the addition of three new energy curves. The first,

TABLE I. Rates of processes diagrammed in Fig. 2.

Process	Rate ^a
${}^7F \rightarrow$ CTS excitation	G
CTS $\rightarrow {}^5D$ feeding	$A = ap_0$
${}^5D \rightarrow$ CTS quenching	$A^{-1} = a^{-1}n_D$
${}^5D \rightarrow {}^7F$ emission	$B = bn_D$
CTS dissociation	$C = \sigma_{p0}v_T\bar{p}_0\bar{p}_0$
Free-hole capture by Eu^{+2}	$C^{-1} = \sigma_{p0}v_T\bar{n}_0\bar{p}$
Trapping of free holes ^b	$D = \sum_i D_i = \sum_i \sigma_{pi}v_T\bar{n}_i\bar{p}$
Detrapping of holes ^b	$D^{-1} = \sum_i D_i^{-1} = \sum_i \sigma_{pi}v_T\bar{p}_i\bar{p}_i$
Loss ^b	$E = \sum_i E_i = \sum_i e_i\bar{p}_i\bar{n}_0$
Eu^{+2} dissociation	$F = \sigma_{n0}v_T\bar{n}_0\bar{p}_0$
Free-electron capture by Eu^{+3}	$F^{-1} = \sigma_{n0}v_TN_{\text{Eu}}n$

^aSteady-state quantities are designated by adding the subscript ∞ . The quantities A^{-1} , a^{-1} , C^{-1} , D^{-1} , and F^{-1} refer to inverse processes and are not numerical inverses of A , a , C , D , and F .

^bThe index i in the rates D , D^{-1} , and E runs over hole traps of all types i . The subscripts $1i$ and $2i$ are used to differentiate between traps that are shallow and deep, respectively. See Appendix A.

TABLE II. Notation for quantities used in Table I.

Quantity ^a	Symbol
[CTS]	p_0
[Eu ⁺²]	n_0
[Hole traps of type i]	N_i
[Holes in traps of type i]	p_i
[Empty traps of type i]	n_i
$\sum N_i$	N_{trap}
[Free holes]	p
[Free electrons]	n
Density of states, valence band	N_v
Density of states, conduction band	N_c
$N_v e^{-E_{p0}/kT}$	\bar{p}_0
$N_v e^{-E_{pi}/kT}$	\bar{p}_i
$N_c e^{-E_{n0}/kT}$	\bar{n}_0
[Eu sites]	N_{Eu}
[Populated ⁵ D states]	n_D
Hole binding energy to Eu ⁺² to form CTS	E_{p0}
Hole binding energy to trap i	E_{pi}
Electron binding energy to Eu ⁺³ to form Eu ⁺²	E_{n0}
Hole-capture cross section for Eu ⁺²	σ_{p0}
Hole-capture cross section for trap i	σ_{pi}
Electron-capture cross section for Eu ⁺³	σ_{n0}
Thermal velocity of free carriers	v_T
Rate constant for CTS → ⁵ D feeding	a
Rate constant for ⁵ D → CTS thermal quenching	a^{-1}
Rate constant for ⁵ D → ⁷ F emission	b
Rate constant for nonradiative recombination of Eu ⁺² and holes in traps of type i	e_i

^a[] means concentration.

labeled ${}^7F_0 + e(\infty) + h(\infty)$, represents the system with a free hole and a free electron far from the unexcited Eu⁺³ ion. The second, labeled Eu⁺² + $h(\infty)$, represents the hole at infinity and the electron trapped at the Eu center as Eu⁺² in its ground ⁸S_{7/2} state. The third, dotted and labeled ${}^7F_0 + e(\vec{r}) + h(\infty)$, represents the hole again at infinity but the electron at some intermediate distance \vec{r} from the unexcited Eu⁺³ ion.

The CTS energy curve was accurately placed relative to the 7F_0 ground-state curve in Ref. 4. It is Franck-Condon shifted relative to the 4*f* states, and its minimum lies 24 000 cm⁻¹ above the 7F_0 minimum in La₂O₂S and 25 100 cm⁻¹ above in Y₂O₂S.

The ${}^7F_0 + e(\infty) + h(\infty)$ energy curve lies one host band-gap energy directly above the 7F_0 ground-state

curve. This band-gap energy is ~35 000 cm⁻¹ for La₂O₂S and ~37 000 cm⁻¹ for Y₂O₂S.

The Eu⁺² + $h(\infty)$ energy curve has its minimum a hole-binding energy E_{p0} above the CTS minimum. Analysis of experimental data in Sec. V will show this binding energy E_{p0} to be 1300 cm⁻¹ for La₂O₂S and 900 cm⁻¹ for Y₂O₂S. The equilibrium configuration of the Eu⁺² + $h(\infty)$ curve lies intermediate between those of the CTS and the 7F_0 curves. This positioning results because Eu⁺² - S⁻² attractions [${}^7F_0 + e(\infty)$ curve] are intermediate between Eu⁺² - S⁻¹ attractions (CTS curve) and Eu⁺³ - S⁻² attractions (7F_0 curve). The exact horizontal position of the Eu⁺² + $h(\infty)$ curve cannot be deduced from the measurements here. Transitions between the CTS and the Eu⁺² + $h(\infty)$ states proceed via a set of intermediate states Eu⁺² + $h(\vec{r})$ with intermediate \vec{r} 's. These intermediate states are not shown in Fig. 3.

The dotted ${}^7F_0 + e(\vec{r}) + h(\infty)$ energy curve is one of a family of curves for different \vec{r} 's. The members of this family are all displaced horizontally from the ${}^7F_0 + e(\infty) + h(\infty)$ curve. Their common minimum energy results because the differential interaction of a free electron with a substitutional Eu⁺³ impurity

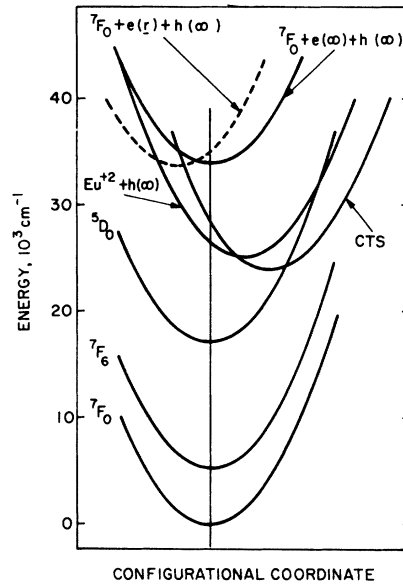


FIG. 3. Configurational-coordinate diagram for the Eu center in La₂O₂S host. Figure shows energy curves for the Eu⁺³ 4*f*⁶ states (⁷F, ⁵D), the lowest Eu⁺³ charge-transfer state (CTS), the state formed by dissociation of the CTS into Eu⁺² and a free hole, the state formed by oxidizing Eu⁺² to Eu⁺³ and a free electron, and one of the intermediate states through which this oxidation proceeds (dotted curve). Luminescence under band-gap excitation proceeds in the reverse sequence ${}^7F_0 \rightarrow {}^7F_0 + e(\infty) + h(\infty) \rightarrow {}^7F_0 + e(\vec{r}) + h(\infty) \rightarrow \text{Eu}^{+2} + h(\infty) \rightarrow \text{CTS} \rightarrow {}^5D \rightarrow {}^7F$. The Eu⁺³ 4*f*⁶ states between 7F_0 and 7F_6 and above ⁵D₀ have been omitted for convenience.

is very short ranged. The particular dotted ${}^7F_0 + e(\vec{r}) + h(\infty)$ curve in Fig. 3 represents that state whose crossover with the $\text{Eu}^{+2} + h(\infty)$ curve is exercised during both electron capture into the Eu^{+3} center and electron release from the Eu^{+2} center. This crossover presents the smallest energy barrier for both electron capture and release. This dotted curve, displaced oppositely from the $\text{Eu}^{+2} + h(\infty)$ curve, is expected for an electron approaching the Eu^{+3} from a nearby La on the opposite side of the S plane.

The electron binding energy E_{n0} for the Eu^{+2} species is the energy difference from the minimum of the $\text{Eu}^{+2} + h(\infty)$ curve to the crossover of this curve with the dotted ${}^7F_0 + e(\vec{r}) + h(\infty)$ curve. For the band-gap, CTS, and E_{p0} energies quoted above, this E_{n0} difference is 9500 cm^{-1} for $\text{La}_2\text{O}_2\text{S}$ and 10700 cm^{-1} for $\text{Y}_2\text{O}_2\text{S}$. The Eu^{+2} lifetime against thermal dissociation into Eu^{+3} and a free electron is (see Tables I and II)

$$\tau = (\sigma_{n0} v_T \bar{n}_0)^{-1} \sim 10^{-11} e^{E_{n0}/kT} \text{ sec} \quad (1)$$

for a non-Coulombic cross section $\sigma_{n0} \sim 10^{-15} \text{ cm}^2$ (electron capture at Eu^{+3}), $v_T \sim 10^7 \text{ cm sec}^{-1}$, and $\bar{n}_0 \sim 10^{19} \text{ cm}^{-3}$. This lifetime is 1 sec at 540 and 610°K for $\text{La}_2\text{O}_2\text{S}$ and $\text{Y}_2\text{O}_2\text{S}$, respectively. Because of this high Eu^{+2} stability, it is possible for energy stored as Eu^{+2} and trapped holes to be recovered at the Eu sites and to be released as $\text{Eu}^{+3} {}^5D \rightarrow {}^7F$ line emissions up to high temperatures. For example, for suitably emptying hole traps, phosphorescence lasting seconds or longer would be observed to the temperatures cited, and thermally or IR-stimulated glow peaks to slightly lower temperatures.

III. EXPERIMENTAL

The materials and apparatus used in this work were described in Refs. 1 and 5.

For $\text{Y}_2\text{O}_2\text{S}:0.1\% \text{Eu}$ and $\text{La}_2\text{O}_2\text{S}:0.5\% \text{Eu}$ under CTS excitation, total ${}^5D \rightarrow {}^7F$ emission was insensitive to temperature up to 500 and 430°K , respectively.⁵ For higher Eu concentrations, this range of constant emission intensity was restricted to lower temperatures, and, above this range, total emission fell off with increasing temperature. We interpret this behavior to mean that, following CTS excitation, total ${}^5D \rightarrow {}^7F$ quantum efficiency is unity in the low-temperature range and falls off at higher temperature. The temperature-insensitive emission at low temperatures was therefore used in this work as a measure of the CTS excitation strength G .

Emission intensity B was expressed in units of photomultiplier output current for the strong ${}^5D_0 \rightarrow {}^7F_2$ emission line ($626 \text{ m}\mu$ for $\text{Y}_2\text{O}_2\text{S}$, $624 \text{ m}\mu$ for $\text{La}_2\text{O}_2\text{S}$). The CTS excitation intensity G was expressed as the photomultiplier output current which would have resulted for this strong ${}^5D_0 \rightarrow {}^7F_2$ emis-

sion line if the total quantum efficiency (all ${}^5D \rightarrow {}^7F$ emissions) had been unity. The relation between the strong ${}^5D_0 \rightarrow {}^7F_2$ emission line and total ${}^5D \rightarrow {}^7F$ emissions had been determined as a function of temperature previously.⁵ Thus, although B and G are both stated for the strong ${}^5D_0 \rightarrow {}^7F_2$ emission line, their ratio B/G is the total quantum efficiency.

A photomultiplier output current of 10^{-9} A corresponded to a ${}^5D_0 \rightarrow {}^7F_2$ emission strength of $\sim 2 \times 10^{10}$ photons sec^{-1} . The sample volume excited was $\sim 10^{-3} \text{ cm}^3$.

IV. RESULTS

In Figs. 4 and 5, rise curves of $\text{La}_2\text{O}_2\text{S}:\text{Eu} {}^5D_0 \rightarrow {}^7F_2$ ($624 \text{ m}\mu$) emissions are given for CTS ($370 \text{ m}\mu$) excitation at high temperature. Data for two concentrations of Eu are shown, each at the several excitation intensities G given in the figures. Before each excitation, the phosphor was exhausted of storage by annealing at the measurement temperature. The initial emission efficiency B_0/G is insensitive to G . The steady-state efficiency B_∞/G gradually shifts from near B_0/G at low G towards unity at high G . The rise times of the slow buildups decrease somewhat with increasing G (Fig. 4) but not so rapidly as $1/G$ (Fig. 5).

Similar rise curves were obtained for $\text{La}_2\text{O}_2\text{S}:2\% \text{Eu}$ and $\text{Y}_2\text{O}_2\text{S}:0.1\% \text{Eu}$ and $2\% \text{Eu}$. These curves all showed the initial efficiency B_0/G to be independent of the excitation intensity G and of the Eu concentration and to decrease from near unity at low temperatures to about 0.1 at 500°K . Some of these B_0/G data will be shown below. For the 2% concentrations the steady-state emission efficiency B_∞/G

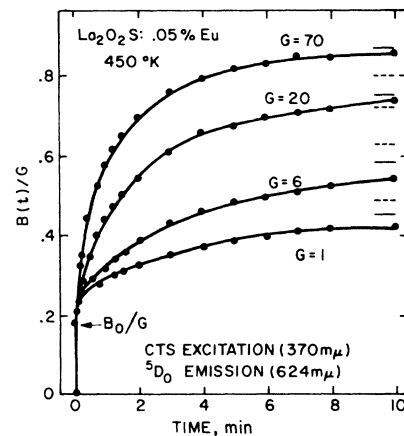


FIG. 4. Rise curves of ${}^5D_0 \rightarrow {}^7F_2$ emission of $\text{La}_2\text{O}_2\text{S}:0.05\% \text{Eu}$ for CTS excitation. The line segments at the right show the observed (solid) and fitted (dotted) steady-state quantum efficiencies B_∞/G . The dotted values were calculated from Eq. (7) with $f'_{\text{feed}} = B_0/G = 0.18$, $\beta = 3.6 \times 10^{-10} \text{ A}$, and $\gamma = 0$. The excitation intensity G is given in units of 10^{-10} A .

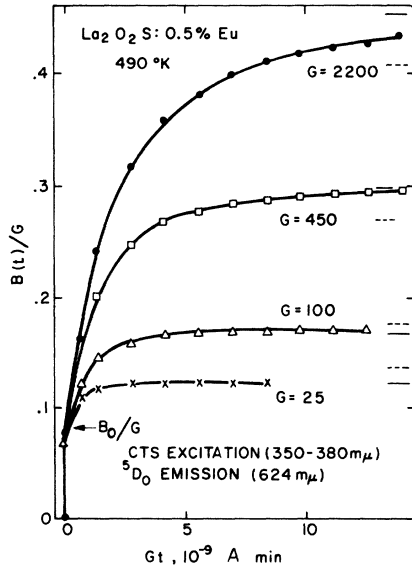


FIG. 5. Rise curves of ${}^5D_0 \rightarrow {}^7F_2$ emissions of $\text{La}_2\text{O}_2\text{S}: 0.5\% \text{Eu}$ for CTS excitation. The abscissa is excitation intensity $G \times \text{time}$. As in Fig. 4, the solid and dotted line segments show observed and fitted steady-state quantum efficiencies B_∞/G . The latter were calculated from Eq. (7) with $f'_{\text{feed}} = B_0/G = 0.085$, $\beta = 1.2 \times 10^{-8} \text{A}$, and $\gamma = 0$. The excitation intensity G is given in units of 10^{-10}A .

increased with G at high temperature (as in Figs. 4 and 5) from near B_0/G at low G towards unity at high G . As already cited in Sec. III, the steady-state efficiency B_∞/G for $\text{Y}_2\text{O}_2\text{S}: 0.1\% \text{Eu}$ was unity up to 500°K .

In Fig. 6, temperature dependences of the steady-state ${}^5D_0 \rightarrow {}^7F_2$ emission are given for $\text{La}_2\text{O}_2\text{S}: 2\% \text{Eu}$ for CTS excitation at four incident flux intensities. At low temperatures where B_0/G and B_∞/G are both near unity, the emission is linear with excitation. At high temperatures, the emission decreases with increasing temperature, and, as the excitation intensity increases, this decrease is postponed to progressively higher temperatures, making the extent of the decrease smaller at any specific temperature. Thus, the high-temperature emission is superlinear with excitation intensity, just as shown previously in Figs. 4 and 5 for 0.05% and 0.5% material. For example, B_∞/G in Fig. 6 increases at 485°K from 0.12 at $G = 21$ to 0.24 at $G = 5500$.

In Fig. 7, the increase of B_∞/G towards unity with increasing excitation intensity G is shown for $\text{Y}_2\text{O}_2\text{S}: 1\%$ and $2\% \text{Eu}$ at a few high temperatures.

In Figs. 8 and 9, the decrease of B_0/G with increasing temperature is shown for $\text{Y}_2\text{O}_2\text{S}$ and $\text{La}_2\text{O}_2\text{S}$, respectively. These data are given in the upper portions of the figures. For each data point, B_0/G was measured from the rise curve of the

phosphor previously exhausted by annealing at 500°K . Points are shown for three concentrations of Eu in $\text{La}_2\text{O}_2\text{S}$, and B_0/G does not depend upon the Eu concentration.

The lower-left portions of Figs. 8 and 9 show storage data for $\text{Y}_2\text{O}_2\text{S}: 0.1\% \text{Eu}$ and $\text{La}_2\text{O}_2\text{S}: 0.5\% \text{Eu}$, respectively. These data were given previously in Ref. 1 and show areas under the 250°K glow peak (including phosphorescence) in these materials after a fixed dosage of CTS excitation at abscissa temperature. In the figures here, these data have been normalized by dividing the glow area by the excitation dosage.

As the temperature during excitation was increased through 250°K , the storage became more temporary, and most of the stored energy was released as delayed Eu^{+3} emissions during the excitation period. The crosses in Fig. 9 show estimated total storage including this temporary storage for $\text{La}_2\text{O}_2\text{S}: 0.5\% \text{Eu}$. These crosses were obtained by adding to the measured glow area the product of the phosphorescence level immediately following excitation multiplied by the length of the excitation period.

Figure 10 shows the phosphorescence of $\text{Y}_2\text{O}_2\text{S}: 1\% \text{Eu}$ at 415°K for three excitation intensities. The excitation times were long enough that the phos-

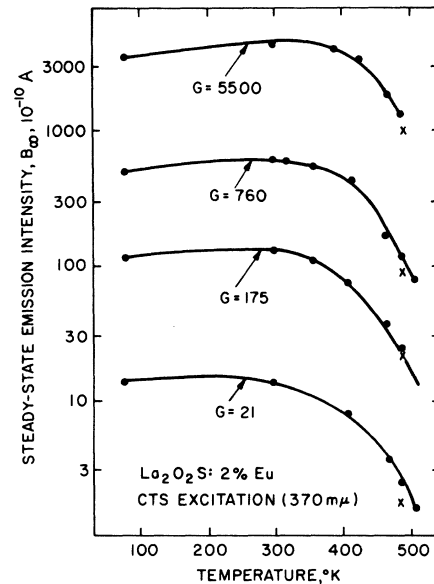


FIG. 6. Temperature dependences of the steady-state ${}^5D_0 \rightarrow {}^7F_2$ emission of $\text{La}_2\text{O}_2\text{S}: 2\% \text{Eu}$ for CTS excitation at four incident flux intensities. For each incident flux intensity, the CTS excitation intensity G increased slightly with increasing temperature. Quoted G values give G at 485°K . Crosses show steady-state emissions at 485°K calculated from Eq. (7) with $f'_{\text{feed}} = 0.085$, $\beta = 6.5 \times 10^{-5} \text{A}$, and $\gamma = 0$.

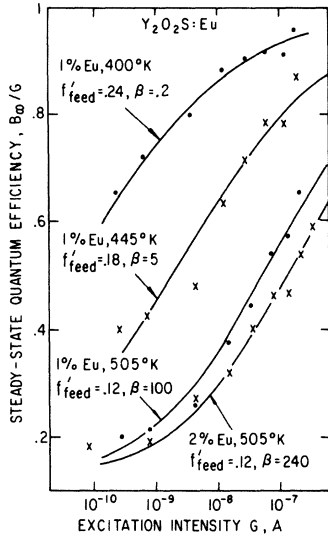


FIG. 7. Steady-state quantum efficiency B_0/G for two $\text{Y}_2\text{O}_2\text{S}:\text{Eu}$ phosphors vs excitation intensity G . Curves fitted to the data points were calculated from Eq. (7) with $\gamma = 0$ and the f'_{feed} and β values given. The f'_{feed} values were fixed by the $\text{Y}_2\text{O}_2\text{S}:\text{Eu}$ $f'_{\text{feed}}(T)$ dependence given in Fig. 8. β values are in units of 10^{-9} A.

phorescence during the 30-sec observation period was insensitive to longer excitation. The phosphorescence is sublinear with excitation intensity. The three curves in Fig. 10 span an intensity range of ~ 15 , whereas the excitation intensity covers a range of ~ 30 .

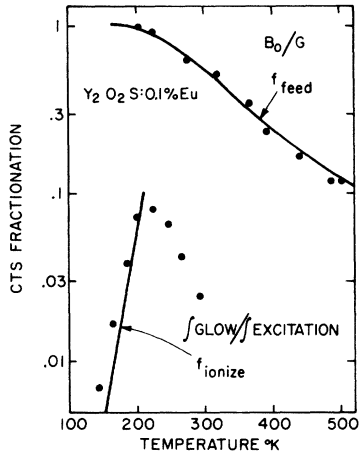


FIG. 8. Temperature dependence of the fractionation of the Eu^{+3} CTS in $\text{Y}_2\text{O}_2\text{S}:0.1\%\text{Eu}$. Upper data points show the initial quantum efficiency $B_0(T)/G$. Lower-left data points give areas under the 250 K glow peak (including phosphorescence) following a fixed CTS excitation dosage at abscissa temperature. f_{feed} and f_{ionize} curves fitted to the data points were calculated from Eqs. (2) and (3) for CTS fractionation with parameter values given in Table III.

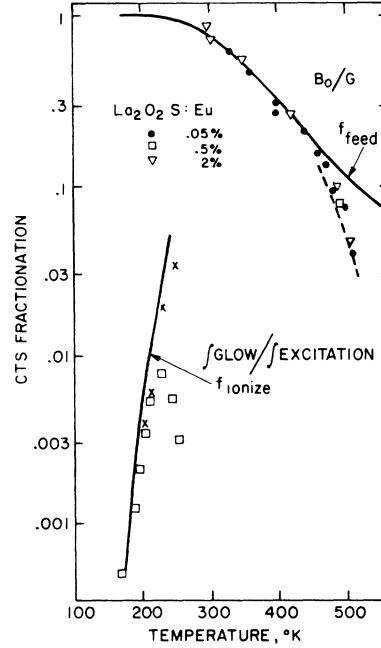


FIG. 9. Temperature dependence of the fractionation of the Eu^{+3} CTS in $\text{La}_2\text{O}_2\text{S}:0.05, 0.5, \text{ and } 2\%\text{Eu}$. As in Fig. 8, the upper data points show $B_0(T)/G$, and the lower-left data points show integrated storage. Squares in the lower left give areas under the IR-stimulated glow peak (including phosphorescence) following a fixed CTS excitation dosage at abscissa temperature. Crosses give total integrated storage, including temporary storage released during the excitation period. f_{feed} and f_{ionize} curves fitted to the data points were calculated from Eqs. (2) and (3) with parameter values given in Table III. Dotted curve shows an improved fit to $B_0(T)/G$ near 500 K. This curve included allowance for 5D_0 quenching and was calculated from Eq. (5).

V. CTS DISSOCIATION

The CTS population p_0 relaxes via $\text{CTS} \rightarrow {}^5D$ feeding at the rate ap_0 (see Table I) and via CTS dissociation at the thermally activated rate $\sigma_{p0}v_T\bar{p}_0p_0$. Therefore, the fraction of CTS excitations which feed the 5D states is

$$f_{\text{feed}} = [1 + (\sigma_{p0}v_T N_v/a)e^{-E_p/kT}]^{-1}, \quad (2)$$

and the fraction which dissociate is

$$f_{\text{ionize}} = 1 - f_{\text{feed}}. \quad (3)$$

If processes A^{-1} and C^{-1} in Fig. 2 are zero, then

$$B = A = f_{\text{feed}}G, \quad C = f_{\text{ionize}}G. \quad (4)$$

At the onset of excitation of a phosphor previously exhausted of Eu^{+2} , C^{-1} is zero. Thus, for such an exhausted phosphor, except for complications due to A^{-1} which will be discussed below, the initial quantum efficiency B_0/G is equal to f_{feed} , and the

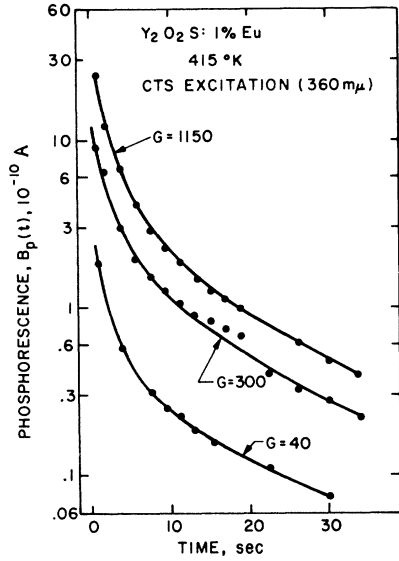


FIG. 10. Phosphorescence of $\text{Y}_2\text{O}_2\text{S}:1\% \text{Eu}$ at 415°K for three excitation intensities. Excitation intensities G are given in units of 10^{-10}A .

initial storage efficiency C_0/G is equal to f_{ionize} .

The functions f_{feed} and f_{ionize} have been fitted to the B_0/G and normalized storage data given for $\text{Y}_2\text{O}_2\text{S}$ and $\text{La}_2\text{O}_2\text{S}$ in Figs. 8 and 9 (solid curves through experimental points). The fitting of f_{ionize} requires that the normalized storage data measure the initial storage efficiency C_0/G ; this point will be discussed below. The f_{feed} and f_{ionize} functions were fitted with the empirical $\sigma_{p0}v_T N_v/a$ and E_{p0} values given in Table III. When A^{-1} processes were taken into account, as discussed below, smaller values of these parameters resulted. These smaller, more correct values are also given in Table III (values in parentheses).

The CTS- 5D feeding rate a had been determined previously⁵ to be $\sim 10^{11.5} \text{sec}^{-1}$ by fitting quenching theory to measured quenchedings of the 5D emissions. Thus, the CTS dissociation constant $\sigma_{p0}v_T N_v$ is here determined to be $\sim 10^{13.5} \text{sec}^{-1}$ for both hosts. This value is in approximate agreement with that estimated for a Coulombic cross section $\sigma_{p0} \sim 10^{-12} \text{cm}^2$ (hole capture at Eu^{+2}), $v_T \sim 10^7 \text{cm sec}^{-1}$, and $N_v \sim 10^{19} \text{cm}^{-3}$. The empirical hole-binding energies E_{p0} given in Table III also agree with an order-of-magnitude estimate, namely, the potential energy of a hole at one Eu-S distance from a Eu^{+2} ion: $e^2/\kappa r \sim 4000 \text{cm}^{-1}$ for $\kappa \sim 10$ and $r \sim 3 \text{\AA}$.

In the low-temperature region where f_{ionize} was fitted to the storage data, both f_{ionize} and losses E were small. Because f_{ionize} was small, C did not change much from its initial value C_0 . Because E was small, the integrated storage $\int C dt$ was fully

recoverable. Thus, the f_{ionize} fit in Figs. 8 and 9 is justified to the extent that the observed storage data do indeed measure total storage. However, as the temperature during excitation was raised through 250°K , appreciable storage was released during the excitation period and was not measured in the glow data reported in Figs. 8 and 9. In this temperature range, the measured glow data fall below f_{ionize} . As cited in Sec. IV, the crosses in Fig. 9 give the estimated total storage, including the temporary storage released during the excitation period. These crosses are in good agreement with fitted f_{ionize} .

The effect of the A^{-1} processes will now be considered. The individual 5D states quench precipitously to the CTS in the order 5D_3 , 5D_2 , 5D_1 , and 5D_0 with increasing temperature.^{4,5,9}

When 5D_0 is not quenched, the 5D states can be grouped into quenched and unquenched states, and the canceling A and A^{-1} processes between the CTS and the quenched 5D states can be ignored. The discussion above predicated upon $A^{-1} = 0$ can then be applied to the unquenched 5D states. That is, B_0/G and C_0/G can be identified with effective CTS fractionation rates. These effective fractions f'_{feed} and f'_{ionize} are given by Eqs. (2) and (3) with the constant a in these equations replaced by a constant a' , giving the partial CTS feeding rate into the unquenched 5D states.

The parameter a' , unlike the parameter a , has a temperature dependence: It decreases below a as the 5D states sequentially quench. We approximated $a'(T)$ as $\frac{1}{4}(j+1)a$, where j is the j of the highest unquenched 5D_j state at T , and fitted the effective fractions f'_{feed} and f'_{ionize} to the B_0/G and storage data in Figs. 8 and 9. This more correct procedure yielded as good a fit to the experimental data as the unprimed curves shown in Figs. 8 and 9, and yielded the more correct $\sigma_{p0}v_T N_v/a$ and E_{p0} values given in parentheses in Table III.

When 5D_0 is quenched ($\text{La}_2\text{O}_2\text{S}$ near 500°K in the work here), the exponential temperature increase of A^{-1} must be explicitly taken into account. B_0/G can still be identified with an effective feeding fraction f'_{feed} given by

TABLE III. Parameters describing CTS dissociation in oxysulfides. The larger values were used to fit f_{feed} and f_{ionize} , given by Eqs. (2) and (3), to the data points in Figs. 8 and 9. The smaller values, in parentheses, are more correct values used to fit the same data taking A^{-1} processes into account.

	$\sigma_{p0}v_T N_v/a$	$E_{p0} (\text{cm}^{-1})$
$\text{Y}_2\text{O}_2\text{S}$	230 (45)	1200 (900)
$\text{La}_2\text{O}_2\text{S}$	900 (75)	1700 (1300)

$$f'_{\text{feed}} = \left\{ 1 + [(\sigma_{p0} v_T N_v / a') e^{-E_{p0}/kT}] [1 + (a'/b') e^{-E'/kT}] \right\}^{-1}, \quad (5)$$

where a' is the partial CTS feeding rate to 5D_0 , b' is the 5D_0 emission rate to the 7F states, and E' is the 5D_0 -to-CTS activation energy.

The dotted curve near 500 °K in Fig. 9 is f'_{feed} as given by Eq. (5). This dotted curve more correctly accounts for the decrease of the observed $\text{La}_2\text{O}_2\text{S } B_0/G$ values near 500 °K. Equation (5) was calculated using $\sigma_{p0} v_T N_v / a = 75$, $a' = \frac{1}{4}a$, $E_{p0} = 1300 \text{ cm}^{-1}$, $a'/b' = 10^8$, and $E' = 6300 \text{ cm}^{-1}$. The $\sigma_{p0} v_T N_v / a$ and a'/a values were consistent with the $\sigma_{p0} v_T N_v / a$ value and $a'(T)/a$ dependence used, as cited above, for fitting the data at temperatures where 5D_0 is not quenched. The $a'b'$ and E' values were given previously for $\text{La}_2\text{O}_2\text{S } {}^5D_0$ quenching in Table II of Ref. 5.

In summary, the B_0/G and storage data shown in Figs. 8 and 9 are both fit by CTS dissociation occurring at a rate described by a rate constant $\sigma_{p0} v_T N_v \sim 10^{13.5} \text{ sec}^{-1}$ and an activation energy $E_{p0} = 900 \text{ cm}^{-1}$ for $\text{Y}_2\text{O}_2\text{S}$, 1300 cm^{-1} for $\text{La}_2\text{O}_2\text{S}$.

At any given temperature, the proportionating of the CTS between emission and dissociation is given by $B/C = f'_{\text{feed}}/f'_{\text{ionize}}$ at all times, not just at the onset of excitation as used in this section. Thus, since $B+C = G + C^{-1}$ (see Fig. 2),

$$B = f'_{\text{feed}}(G + C^{-1}), \quad C = f'_{\text{ionize}}(G + C^{-1}). \quad (6)$$

These relations will be used in later sections.

VI. SUPERLINEAR TRANSITION OF STEADY-STATE EMISSION WITH EXCITATION INTENSITY

Although the initial quantum efficiency $B_0(T)/G$ is independent of the Eu concentration and of the excitation intensity G , the steady-state quantum efficiency B_∞/G has complex dependences. B_∞/G ranges from $B_0(T)/G$ to unity. It tends towards the unity limit for low temperature, low Eu concentration, and high excitation intensity; and towards the $B_0(T)/G$ limit for high temperature, high [Eu], and low G (see Figs. 4-7).

These behaviors suggest that the emission B be viewed as consisting of two components. One component $B_0(T)$ arises from a fixed fraction $B_0(T)/G$ of the excitations being emitted immediately without loss. The other component $B - B_0(T)$, which builds up from zero as storage accumulates, arises from the remaining fraction of the excitations being emitted only after having been subjected to storage-induced, temperature-, Eu-concentration-, and intensity-dependent losses.

In the model presented in Secs. II and V, the component $B_0(T)$ results from the component $f'_{\text{feed}} \times G$ of the excitations which follow the direct deexcitation path $\text{CTS} \rightarrow {}^5D \rightarrow {}^7F$. The component $B - B_0(T)$ arises from the component $f'_{\text{ionize}} G$ of the excita-

tions which undergo CTS dissociation. The buildup of the $B - B_0(T)$ component is associated with the buildup of storage in the previously exhausted phosphor. The rate of CTS reformations (process C^{-1} in Fig. 2) builds up from zero as the Eu^{+2} concentration builds up. Consequently, the CTS concentration p_0 increases from an initial value that supports $B_0 = f'_{\text{feed}} G$ to a final value that supports $B_\infty = f'_{\text{feed}}(G + C_\infty^{-1})$.

The $B_\infty - B_0 = f'_{\text{feed}} C_\infty^{-1}$ depends superlinearly on the excitation G because of competition for free holes between the loss-process sequence D , E and the CTS reformation process C^{-1} . At high temperatures, high Eu concentration, and low excitation intensity, most of the $f'_{\text{ionize}} G$ holes generated per unit time are trapped and are dissipated nonradiatively. The emission intensity therefore remains near the initial emission intensity $B_0(T) = f'_{\text{feed}} G$. At low T , low [Eu] and high G , the rate C^{-1} of CTS reformations builds up during excitation and tends to cancel the rate C of CTS dissociations. The emission rate B is then near the excitation rate G .

A quantitative relation between B_∞ and G has been derived in Appendix A. This derivation used the rates listed in Table I with the approximations that the Eu^{+2} concentration n_0 is charge balanced by the trapped-hole charge; the traps can be divided into two types, shallow traps (type 1) kept mostly empty by detrapping ($D_{1i} \approx D_{1i}^{-1}$) and deeper traps (type 2) kept mostly empty by loss ($D_{2i} \approx E_{2i}$); and most of the loss occurs through the deeper traps ($E \approx E_2 = \sum_i E_{2i}$). The relation between B_∞ and G is conveniently stated through a parametric variable $\hat{n}_{0\infty}$ that increases sublinearly with excitation intensity:

$$G = \frac{1}{2}\beta(1 + \gamma)(\hat{n}_{0\infty}^3 + \hat{n}_{0\infty}^2)/(1 + \gamma \hat{n}_{0\infty}), \quad (7)$$

$$\frac{B_\infty}{G} = f'_{\text{feed}} + \frac{\hat{n}_{0\infty}}{(1 + \hat{n}_{0\infty})} f'_{\text{ionize}}.$$

The $\hat{n}_{0\infty}$, defined as $f'_{\text{feed}} C_\infty^{-1}/D_{2\infty}$, is the ratio of the probability that a free hole will generate emission (sequence C^{-1} , A , B) to the probability that it will be trapped in deep traps and lost (sequence D_{2i} , E). The $\hat{n}_{0\infty}$ is proportional to the steady-state Eu^{+2} concentration $n_{0\infty}$ and can be regarded as a scaled Eu^{+2} concentration. At any given temperature, β , γ , f'_{feed} , and f'_{ionize} are constants.

As $\hat{n}_{0\infty}$ increases sublinearly with G , B_∞/G undergoes a gradual rise from its limit $f'_{\text{feed}} = B_0/G$ for $\hat{n}_{0\infty} \ll 1$ to its limit $f'_{\text{feed}} + f'_{\text{ionize}} = 1$ for $\hat{n}_{0\infty} \gg 1$. The B_∞/G passes through the mean $f'_{\text{feed}} + \frac{1}{2} f'_{\text{ionize}}$ of its limits at $\hat{n}_{0\infty} = 1$, $G = \beta$. Figure 11 shows gradual $B_\infty(G)$ transitions computed from Eq. (7) for several values of f'_{feed} and for $\gamma = 0$ (solid curves) and 1 (dotted curves). These transitions are somewhat less gradual for $\gamma = 1$.

The parameters β and γ are defined in Appendix

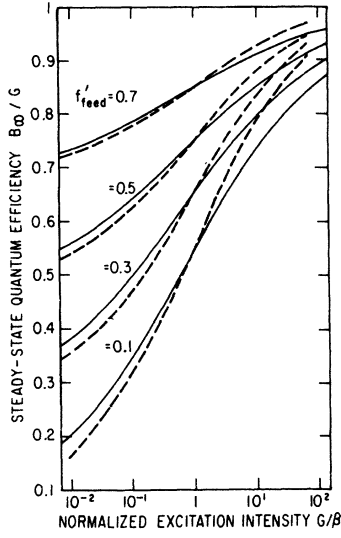


FIG. 11. Superlinear transition of steady-state emission B_∞ vs excitation G calculated from the model of the CTS dissociating into Eu^{+2} and a free hole. These curves were calculated from Eq. (7) and give the steady-state quantum efficiency B_∞/G as a function of the scaled excitation intensity G/β . Solid curves are for $\gamma=0$ (deep traps only); the dotted curves are for $\gamma=1$ (shallow and deep traps).

A. β is proportional to the rate constants e_{2i} for nonradiative recombination of Eu^{+2} and holes in deep traps, and increases with temperature and Eu concentration through these constants. Since $G=\beta$ when $\hat{n}_{0\infty}=1$, β is the excitation intensity that establishes the steady-state Eu^{+2} concentration $n_{0\infty}$ for which free holes lead with equal probability to emission and loss. The parameter γ contains all effects of the shallow traps; when such traps are absent, $\gamma=0$. The $\gamma\hat{n}_{0\infty}$ is the ratio of charge stored in shallow traps to charge stored in deep traps.

Equation (7) has been fitted to the $B_\infty(G)$ data in Figs. 4–7 for $\gamma=0$ (no shallow traps). The fitted values are the dotted levels at the right edges of Figs. 4 and 5, the crosses in Fig. 6, and solid curves in Fig. 7. The f'_{feed} and β values used in the fittings are given in the figure captions. At each temperature, f'_{feed} was taken equal to $B_0(T)/G$ as given in Fig. 8 for $\text{Y}_2\text{O}_2\text{S}$ and in Fig. 9 for $\text{La}_2\text{O}_2\text{S}$. The β values were adjusted empirically for good fit. The empirical β values increase with increasing T and $[\text{Eu}]$, as expected because of increased electron hopping among the Eu sites (increased e_{2i}).

The data can also be fitted by somewhat less gradual transitions given by Eq. (7) for $\gamma>0$. For example, the data in Fig. 7 can be fitted equally well for any γ less than 0.2 for the 400 °K curve and less than 1 for the 505 °K curves.

In summary, observed gradual transitions in quantum efficiency from values near B_0/G at low excitation intensity to values near unity at high excitation intensity are described by Eq. (7). This equation is based on the CTS dissociating into Eu^{+2} and a free hole, and reflects the competition for free holes between the loss sequence D_2 , E and the delayed-emission sequence C^{-1} , A , B .

At high temperatures, the rates C_∞ and C_∞^{-1} of CTS dissociation and reformation can exceed the excitation rate G by a sizable factor ($\sim 1/f'_{\text{feed}}$). This situation arises when B_∞/G is near unity (high G , low $[\text{Eu}]$), as may be seen from Eqs. (6) with $B_\infty \approx G$, $f'_{\text{feed}} \ll 1$.

VII. Eu^{+2} CONCENTRATION n_0 AND RISE TIME

One characteristic of the model is that the steady-state Eu^{+2} concentration $n_{0\infty}$ (and the equal trapped-hole charge $\sum_i p_{i\infty}$) increases sublinearly with excitation intensity G —as the $\frac{1}{2}$ to $\frac{1}{3}$ power of G according to Eq. (7). This sublinear increase stems from the CTS reformation rate C^{-1} increasing as the product $n_0\beta$.

The sublinear increase of stored charge manifests itself in the rise time of slow buildup $B-B_0$. In the model here, a fraction f'_{ionize} of CTS excitations dissociates and becomes apportioned among storage, loss, and delayed emission. At initial excitation of an exhausted phosphor, the loss and delayed-emission components are zero, and the component going into storage is fully $f'_{\text{ionize}}G$. Thereafter, the loss and delayed-emission components build up to steady-state values, and the storage component decreases to zero. Thus, the charge $n_{0\infty}$ stored at steady state is approximated by $\frac{1}{2}f'_{\text{ionize}}G\Delta t_{\text{rise}}$, where Δt_{rise} is the rise time of the buildup. Solving for Δt_{rise} and using \hat{n}_0 as defined in Appendix A, we find that this approximation becomes

$$\Delta t_{\text{rise}} = \frac{2n_{0\infty}}{f'_{\text{ionize}}G} = \frac{2\langle\sigma_{p2i}\rangle N_{2\text{trap}}}{\sigma_{p0}} \frac{\hat{n}_{0\infty}}{f'_{\text{feed}}f'_{\text{ionize}}G}. \quad (8)$$

This formula shows that the rise time Δt_{rise} should decrease with increasing G as the $\frac{1}{2}$ to $\frac{2}{3}$ power of G . In any given case, the exact G dependence can be predicted from exact $\hat{n}_{0\infty}$ values obtained by fitting Eq. (7) to steady-state $B_\infty(G)$ data.

In Fig. 4, rise transients were plotted on a time abscissa t , and Δt_{rise} is seen to decrease with increasing G . In Fig. 5, the rise transients were instead plotted on an excitation-dosage abscissa Gt , and $G\Delta t_{\text{rise}}$ is seen to increase with increasing G . Although not shown, when these rise transients were plotted on the abscissa $t' \equiv f'_{\text{feed}}f'_{\text{ionize}}Gt/\hat{n}_{0\infty}$ suggested by Eq. (8) and intermediate between time and dosage, the transients then exhibited approximately equal rise constants $\Delta t'_{\text{rise}}$. This behavior

is a direct manifestation of the stored charge increasing sublinearly with G .

In the work here, the Eu^{+2} concentration never became larger than $\sim 10^{16} \text{ cm}^{-3}$, which corresponded to $\sim 10^{13} \text{ Eu}^{+2}$ ions in the $\sim 10^{-3}\text{-cm}^3$ sample volume excited. This upper limit came from measured storage areas (either over slow buildup transients or under glow peaks) and the relation between photomultiplier current and photon flux given in Sec. III. Larach and Faughnan of these laboratories looked for but did not find an excitation-induced Eu^{+2} EPR signal in these phosphors. These results are not conclusive, however, because the number of Eu^{+2} spins expected in their experiments might have been below the detection limit.

In contrast with the slow emission buildups associated with storage reported here, Forest, Cocco, and Hersh³ have reported slow emission decreases ($\sim 10\%$) associated with storage in $\text{La}_2\text{O}_2\text{S}:\text{Eu}$. They attributed these emission decreases to reduced Eu^{+3} absorption due to excitation-induced conversion of Eu^{+3} into either Eu^{+2} and a hole or Eu^{+4} and an electron. In the cases here, the excitation produced no more than 10^{16} Eu^{+2} ions per cm^3 and thus negligibly changed the Eu^{+3} concentration.

According to the detailed model developed in Appendix A, the hole traps were always mostly empty of holes. Thus, we believe that the total concentration of hole traps exceeded the 10^{16}-cm^{-3} maximum Eu^{+2} concentration.

VIII. PHOSPHORESCENCE

Slow phosphorescence B_P and slow buildup $B - B_0$ were found to be asymmetric in the sense that initial slow phosphorescence was smaller than total buildup $B_\infty - B_0$ (see Fig. 1). The phosphorescence was also found to be sublinear in the excitation intensity G , varying typically at about $G^{0.7}$. Both asymmetry and sublinearity can be understood from the model of this paper.

The B_P sublinearity comes about as follows. Phosphorescence B_P is a consequence of detrapping D^{-1} through the chain D^{-1} , C^{-1} , A , B (see Fig. 1). In the model here, the Eu^{+2} concentration n_0 and the trapped-hole concentration $\sum_i p_i$ are charge balanced, and both increase sublinearly with excitation intensity G . The D^{-1} is proportional to the p_i 's and therefore increases sublinearly. This sublinear D^{-1} increase becomes translated through the D^{-1} , C^{-1} , A , B chain to a sublinear $B_P(G)$ variation.

Phosphorescence B_P and buildup $B - B_0$ are related because both stem from the chain C^{-1} , A , B . Indeed, initial phosphorescence and total buildup stand in the ratio $B_P(0)/(B_\infty - B_0) = D_\infty^{-1}/(D_\infty^{-1} + f'_{\text{ionize}}G)$. This may be seen as follows. Since detrapping D^{-1} and excitation G generate free holes at the rates D^{-1} and $f'_{\text{ionize}}G$, respectively, the free-hole concentration p can be regarded as a superposition of

component concentrations $p_{D^{-1}}$ and p_G generated by detrapping D^{-1} and excitation G and proportional to D^{-1} and $f'_{\text{ionize}}G$, respectively. As the excitation is removed, G and p_G decrease rapidly to zero, but n_0 , D^{-1} , and $p_{D^{-1}}$, associated with stored charge, decrease slowly. Thus, n_0 , D^{-1} , and $p_{D^{-1}}$ have the same values $n_{0\infty}$, D_∞^{-1} , and $p_{D_\infty^{-1}}$ during steady state and at initial phosphorescence. The stated phosphorescence-buildup ratio then follows from the relations

$$\begin{aligned} \frac{B_P(0)}{B_\infty - B_0} &= \frac{C_P^{-1}(0)}{C_\infty^{-1}} = \frac{n_{0P}(0)p_P(0)}{n_{0\infty}p_\infty} = \frac{p_P(0)}{p_\infty} = \frac{p_{D_P^{-1}}(0)}{p_{D_\infty^{-1}} + p_G} \\ &= \frac{p_{D_\infty^{-1}}}{p_{D_\infty^{-1}} + p_G} = \frac{D_\infty^{-1}}{D_\infty^{-1} + f'_{\text{ionize}}G} \end{aligned}$$

The phosphorescence-buildup ratio is thus small to the extent that D_∞^{-1} is small compared to $f'_{\text{ionize}}G$. In the model here, the ratio of D_∞^{-1} to $f'_{\text{ionize}}G$ proves to be a consequence of the proportion of shallow to deep traps and could, *a priori*, be large or small. However, given a suitable shallow-to-deep-trap ratio to make the phosphorescence-buildup ratio small, the model does explain that this ratio becomes smaller with increasing excitation intensity G . This increasing asymmetry follows from the sublinear increase of D_∞^{-1} associated with the sublinear increase of stored charge.

An expression for the slow phosphorescence B_P has been derived in Appendix B. This expression involves two new constants δ and ϵ characterizing detrapping D^{-1} . The δ is the ratio D_1/D_2 ; ϵ , a constant of the deep traps, is $\hat{n}_{0\infty}D_{2\infty}^{-1}/D_{2\infty}$. These two constants are independent of the constants β and γ used previously in Eq. (7) for the steady state. The B_P expression is

$$\begin{aligned} B_P(t) &= \frac{D^{-1}(t)}{1 + (1 + \delta)/\hat{n}_0(t)} \\ &= \frac{\hat{n}_{0\infty} f'_{\text{ionize}} G}{1 + \hat{n}_{0\infty}} \left[\frac{\alpha_1(t)\delta + \alpha_2(t)\epsilon/\hat{n}_{0\infty}}{\hat{n}_{0\infty} + (1 + \delta)/\alpha_0(t)} \right] \end{aligned} \quad (9)$$

The $\hat{n}_{0\infty} f'_{\text{ionize}} G / (1 + \hat{n}_{0\infty})$ is the total buildup ($B_\infty - B_0$) [see Eq. (7)]. The term in square brackets is the phosphorescence-buildup ratio $B_P/(B_\infty - B_0)$. The $\alpha_0(t)$, $\alpha_1(t)$, and $\alpha_2(t)$ decrease slowly from unity. The $\alpha_0(t)$ is the normalized time dependence of the Eu^{+2} concentration $n_0(t)$. The $\alpha_1(t)$ and $\alpha_2(t)$ are the normalized time dependences of the detrapping rates from the shallow traps $D_1^{-1}(t)$, and deep traps $D_2^{-1}(t)$, respectively. The $\alpha_1(t)\delta$ and $\alpha_2(t)\epsilon/\hat{n}_{0\infty}$ are $D_1^{-1}(t)$ and $D_2^{-1}(t)$ in units of $D_{2\infty}$. The denominator in the square brackets is $\hat{n}_{0\infty} + 1 + \delta$ at initial phosphorescence and is then $f'_{\text{ionize}}G + D_\infty^{-1}$ in units of $D_{2\infty}$ [see Eqs. (A6) and (B5) and related text in the Appendices].

TABLE IV. Phosphorescence of $Y_2O_2S:1\%Eu$ at 415 °K. At this temperature, $f'_{\text{ionize}} = 0.78$ for Y_2O_2S . G/β and $\hat{n}_{0\infty}$ were obtained by fitting Eq. (7) to steady-state $B_\infty(G)$ data with $\beta = 5.7 \times 10^{-10}$ A and $\gamma = 0$. Fitted $B_P(t)/G$ values were calculated from Eq. (9) with the parameters given in the table.

	Equation (9) parameters				$G(10^{-10}$ A)		
	α_0	δ	$\delta\alpha_1$	$\epsilon\alpha_2$	40	300	1150
G/β					7.0	53	200
$\hat{n}_{0\infty}$					2.1	4.5	7.0
$(B_\infty - B_0)/G^{\frac{1}{2}}$					0.53	0.64	0.68
	$B_P(2 \text{ sec})/G$						
Observed					0.045	0.030	0.021
Fitted	1	0	0	1.00	0.081	0.026	0.012
	1	1/3	0.24	0.11	0.045	0.029	0.021
	1	2/3	0.24	0.17	0.045	0.029	0.021
	$B_P(15 \text{ sec})/G$						
Observed					0.0039	0.0025	0.0011
Fitted	2/3	0	0	0.080	0.0056	0.0019	0.0009
	2/3	1/3	0.011	0.042	0.0040	0.0020	0.0013
	2/3	2/3	0.011	0.050	0.0040	0.0020	0.0013
	1/3	0	0	0.110	0.0047	0.0019	0.0010
	1/3	1/3	0.011	0.075	0.0040	0.0021	0.0013
	1/3	2/3	0.011	0.090	0.0040	0.0021	0.0014

^aCalculated, using Eq. (7), as $[\hat{n}_{0\infty}/(1 + \hat{n}_{0\infty})] f'_{\text{ionize}}$.

The factor $[1 + (1 + \delta)/\hat{n}_0(t)]^{-1}$ in Eq. (9) is the fraction of detrapping D^{-1} which appears as phosphorescence B_P . This fraction, through \hat{n}_0 , increases with increasing G and thus has the effect of making B_P less sublinear with excitation G than D^{-1} . That is, an observed sublinear B_P increase is direct evidence for an even more sublinear increase of stored charge. The detailed expression for B_P given in Eq. (9) shows B_P increasing as G at low $\hat{n}_{0\infty}$ and as $G/\hat{n}_{0\infty} \propto G^{2/3}$ at high $\hat{n}_{0\infty}$. Observed B_P sublinearities are ascribed to this $B_P(G)$ dependence.

Equation (9) also contains asymmetry to the extent that the phosphorescence–buildup ratio in the square brackets is small. The $\alpha_2(t)\epsilon/\hat{n}_{0\infty}$ is small compared to unity by the definition of deep traps $D_{2\infty}^1 \ll D_{2\infty}$. Thus, the initial phosphorescence–buildup ratio is small if $\delta \ll (1 + \hat{n}_{0\infty})$, that is, if the shallow traps are not too numerous. The observed asymmetries are ascribed to this δ inequality characterizing our materials. The increase of asymmetry with excitation G is ascribed to the effect of increasing $\hat{n}_{0\infty}$ in the square brackets. One detailed fitting of Eq. (9) to observed asymmetry and sublinearity will be described below.

It was shown in Sec. VI that observed gradual B_∞/G -vs- G transitions could be fitted by Eq. (7), assuming either deep traps only ($\gamma = 0$) or both deep and shallow traps ($\gamma > 0$). One might expect that the role of the shallow traps is more important in the phosphorescence. Indeed, although Eq. (9), with deep traps only ($\delta = 0$), leads to a sublinear B_P variation with G , it generally overestimated ob-

served B_P nonlinearities. Equation (9) with both deep and shallow traps was needed to give good fits to observed B_P data.

Table IV gives the results of fitting Eq. (9) to the Fig. 10 phosphorescence data for $Y_2O_2S:1\%Eu$ at 415 °K. G/β , $\hat{n}_{0\infty}$, and buildup $(B_\infty - B_0)/G$ were obtained by interpolating an empirical B_∞/G -vs- G dependence at 415 °K from the $Y_2O_2S:1\%Eu$ data in Fig. 7 and then fitting Eq. (7) to this dependence. For the 2-sec phosphorescence, the phosphorescence–buildup ratio $B_P/(B_\infty - B_0)$ decreased from 0.045/0.53 = 0.085 at $\hat{n}_{0\infty} = 2.1$ to 0.021/0.68 = 0.031 at $\hat{n}_{0\infty} = 7.0$. Because Eq. (7) fitted the B_∞/G data in Fig. 7 well, these ratios are automatically fitted here if Eq. (9) is fitted to the observed phosphorescence.

B_P was fitted to the data assuming deep traps only ($\delta = 0$) and both shallow and deep traps ($\delta > 0$). For the case of deep traps only ($\delta = 0$), Eq. (9) gave a rough fit to the data but overestimated the B_P sublinearity at 2 sec by a factor of 3 across the factor-of-30 G range covered. For both shallow and deep traps ($\delta > 0$), good fits of Eq. (9) to the data were obtained: for δ values in the range $\frac{1}{3} - \frac{2}{3}$, for $\alpha_1(t)\delta$ decreasing from 0.24 at 2 sec to 0.011 at 15 sec, for $\alpha_0(t)$ decreasing from near unity at 2 sec to $\frac{1}{3} - \frac{2}{3}$ at 15 sec, and for $\alpha_2(t)\epsilon$ decreasing from near 0.14 at 2 sec to near 0.06 at 15 sec. Detrapping from the shallow traps dominated the 2-sec phosphorescence, but detrapping from both types of traps contributed comparably to the 15-sec phosphorescence.

The $\alpha_0(t)$ and $\alpha_2(t)$ decreases should become steeper with increasing G because of the product

form $E_i = e_i n_0 p_i$ assumed for losses. Although this effect has been neglected above, $\alpha_0(t)$ and $\alpha_2(t)$ decreases of the bimolecular form $(1 + \alpha \hat{n}_{0\infty} t)^{-1}$ do lead to equally good fits of Eq. (9) to the data.

In summary, gradual B_∞/G -vs- G transitions, asymmetries $B_p/(B_\infty - B_0)$, and sublinearities $B_p(G)$ could all be fitted with the model of the CTS dissociating into Eu^{+2} and a free hole.

IX. CONCLUSIONS

In oxysulfides with Eu^{+3} , excitation into the CTS leads not only to direct CTS \rightarrow 5D feeding but also partially to CTS dissociations into Eu^{+2} and free holes. CTS dissociation proceeds with a rate constant of $\sim 10^{13.5} \text{ sec}^{-1}$ and an activation energy of 900 cm^{-1} in $\text{Y}_2\text{O}_2\text{S}$ and 1300 cm^{-1} in $\text{La}_2\text{O}_2\text{S}$. These constants agree with order-of-magnitude estimates of their values.

CTS excitation of a previously exhausted phosphor leads to a buildup of emissions from an initial value to a steady-state value. The initial quantum efficiency is independent of excitation intensity and of Eu concentration. The steady-state quantum efficiency increases superlinearly with excitation intensity and depends on Eu concentration. The rise time of the buildup decreases sublinearly with excitation intensity. The phosphorescence when excitation is removed is asymmetric with respect to the rise curve and increases sublinearly with excitation intensity. All these behaviors can be fitted with the model of the CTS dissociating into Eu^{+2} and holes and of the recombination of Eu^{+2} s and trapped holes being nonradiative. In this model, the Eu^{+2} and trapped-hole charges stored in the steady state increase sublinearly with excitation, and this sublinear increase is directly manifested in the sublinear decrease of rise time and sublinear increase of phosphorescence with increasing excitation.

APPENDIX A: STEADY-STATE QUANTUM EFFICIENCY

In the steady state (denoted by subscript ∞), the rates in Fig. 2 satisfy the relations

$$G = B_\infty + E_\infty, \quad C_\infty = C_\infty^{-1} + E_\infty, \quad D_\infty = D_\infty^{-1} + E_\infty. \quad (\text{A1})$$

Since

$$B/C = f'_{\text{feed}}/f'_{\text{ionize}}, \quad (\text{A2})$$

it follows that

$$\begin{aligned} G &= \left(\frac{B}{C}\right) C_\infty + E_\infty = \left(\frac{f'_{\text{feed}}}{f'_{\text{ionize}}}\right) (C_\infty^{-1} + E_\infty) + E_\infty \\ &= \left(f'_{\text{feed}} \frac{C_\infty^{-1}}{E_\infty} + 1\right) \frac{E_\infty}{f'_{\text{ionize}}}. \end{aligned} \quad (\text{A3})$$

The approximation is made that the trap-emptying processes D^{-1} and E keep the traps mostly empty of holes ($N_i = n_i + p_i \approx n_i$), that the traps can be divided into two types: shallow traps (1) kept mostly

empty by detrapping ($D_{1i\infty} = D_{1i\infty}^{-1} + E_{1i\infty} \approx D_{1i\infty}^{-1}$) and deep traps (2) kept mostly empty by loss ($D_{2i\infty} = D_{2i\infty}^{-1} + E_{2i\infty} \approx E_{2i\infty}$), and that most losses occur from the deep traps ($E_\infty = E_{1\infty} + E_{2\infty} \approx E_{2\infty} = \sum_i E_{2i\infty}$). Then,

$$\begin{aligned} E_\infty = E_{2\infty} = D_{2\infty} &= \sum_i D_{2i\infty} = \sum_i \sigma_{p2i} v_T N_{2i} p_\infty \\ &= \langle \sigma_{p2i} \rangle v_T N_{2\text{trap}} p_\infty. \end{aligned} \quad (\text{A4})$$

Defining

$$\hat{n}_0 = f'_{\text{feed}} \frac{C^{-1}}{D_2} = f'_{\text{feed}} \frac{\sigma_{p0} n_0}{\langle \sigma_{p2i} \rangle N_{2\text{trap}}}, \quad (\text{A5})$$

one finds that

$$G = [(\hat{n}_{0\infty} + 1)/f'_{\text{ionize}}] E_\infty \quad (\text{A6})$$

and

$$\frac{B_\infty}{G} = 1 - \frac{E_\infty}{G} = \frac{\hat{n}_{0\infty} + f'_{\text{feed}}}{1 + \hat{n}_{0\infty}} = f'_{\text{feed}} + \frac{\hat{n}_{0\infty}}{1 + \hat{n}_{0\infty}} f'_{\text{ionize}}. \quad (\text{A7})$$

When $\hat{n}_{0\infty} = 1$, B_∞/G has the value $f'_{\text{feed}} + \frac{1}{2} f'_{\text{ionize}}$ half-way between its limiting values f'_{feed} for $\hat{n}_{0\infty} \ll 1$ and $f'_{\text{feed}} + f'_{\text{ionize}} = 1$ for $\hat{n}_{0\infty} \gg 1$.

The charge-balance equation ($n_0 = \sum_i p_{1i} + \sum_i p_{2i}$), together with the relations above describing two types of traps, gives

$$p_\infty = \frac{n_{0\infty}^2}{n_{0\infty} \langle 1/\bar{p}_{1i} \rangle N_{1\text{trap}} + \langle \sigma_{p2i}/e_{2i} \rangle v_T N_{2\text{trap}}}. \quad (\text{A8})$$

Defining

$$\begin{aligned} \gamma &= \frac{\langle 1/\bar{p}_{1i} \rangle N_{1\text{trap}} \langle \sigma_{p2i} \rangle}{f'_{\text{feed}} \sigma_{p0} v_T \langle \sigma_{p2i}/e_{2i} \rangle}, \\ \beta &= \frac{2 \langle \sigma_{p2i} \rangle^3 N_{2\text{trap}}^2}{(1 + \gamma) f'_{\text{ionize}} f'_{\text{feed}} \sigma_{p0}^2 \langle \sigma_{p2i}/e_{2i} \rangle}, \end{aligned} \quad (\text{A9})$$

one finds that

$$\begin{aligned} E_\infty = D_{2\infty} &= \langle \sigma_{p2i} \rangle v_T N_{2\text{trap}} p_\infty \\ &= \frac{1}{2} \beta (1 + \gamma) f'_{\text{ionize}} \hat{n}_{0\infty}^2 / (1 + \gamma \hat{n}_{0\infty}) \end{aligned} \quad (\text{A10})$$

and

$$G = \frac{\hat{n}_{0\infty} + 1}{f'_{\text{ionize}}} E_\infty = \frac{1}{2} \beta (1 + \gamma) \frac{\hat{n}_{0\infty}^3 + \hat{n}_{0\infty}^2}{1 + \gamma \hat{n}_{0\infty}}. \quad (\text{A11})$$

When $\hat{n}_{0\infty} = 1$, G has the value β . Equations (A7) and (A11) were cited in the text as Eq. (7).

When no shallow traps are present, $\gamma = 0$, and Eqs. (A7) and (A11) can be combined to give

$$\frac{G}{\beta} = \frac{1}{2} f'_{\text{ionize}} \frac{(B_\infty/G - f'_{\text{feed}})^2}{(1 - B_\infty/G)^3}. \quad (\text{A12})$$

APPENDIX B: PHOSPHORESCENCE

When excitation is removed, $G = 0$, $B = f'_{\text{feed}} C^{-1}$, and $D^{-1} = D + B$, and thus

$$B = \frac{B}{D^{-1}} D^{-1} = \frac{D^{-1}}{(B+D)/B} = \frac{D^{-1}}{1 + D/f'_{\text{feed}} C^{-1}} \quad (\text{B1})$$

Dividing the traps into shallow (1) and deep (2) traps as in Appendix A, the $D/f'_{\text{feed}} C^{-1}$ denominator term becomes

$$\frac{D_1 + D_2}{f'_{\text{feed}} C^{-1}} = \left(\frac{D_1}{D_2} + 1 \right) \frac{D_2}{f'_{\text{feed}} C^{-1}} = \frac{\delta + 1}{\hat{n}_0} \quad (\text{B2})$$

where

$$\delta = \frac{D_1}{D_2} = \frac{\langle \sigma_{p1i} \rangle N_{1\text{trap}}}{\langle \sigma_{p2i} \rangle N_{2\text{trap}}} \quad (\text{B3})$$

The Eu^{*2} concentration $n_0(t)$ and the trapped-hole concentrations decrease slowly when excitation is removed. Thus,

$$\begin{aligned} \hat{n}_0(t) &= \hat{n}_0(0) \alpha_0(t), & D_1^{-1}(t) &= D_1^{-1}(0) \alpha_1(t), \\ D_2^{-1}(t) &= D_2^{-1}(0) \alpha_2(t), \end{aligned} \quad (\text{B4})$$

where $\alpha_0(t)$, $\alpha_1(t)$, and $\alpha_2(t)$ decrease slowly from unity and

$$\begin{aligned} \hat{n}_0(0) &= \hat{n}_{0\infty}, & D_1^{-1}(0) &= D_{1\infty}^{-1} = D_{1\infty} = \delta D_{2\infty}, \\ D_2^{-1}(0) &= D_{2\infty}^{-1} = (\epsilon / \hat{n}_{0\infty}) D_{2\infty}. \end{aligned} \quad (\text{B5})$$

The deep-trap constant ϵ is given by

$$\begin{aligned} \epsilon &\equiv \hat{n}_{0\infty} D_{2\infty}^{-1} / D_{2\infty} \\ &= \langle \sigma_{p2i} \bar{p}_{2i} / e_{2i} \rangle v_T f'_{\text{feed}} \sigma_{p0} / \langle \sigma_{p2i} \rangle^2 N_{2\text{trap}}. \end{aligned} \quad (\text{B6})$$

The slow-time dependences $\alpha_0(t)$, $\alpha_1(t)$, and $\alpha_2(t)$ will not need to be known accurately since our main concern lies with the G dependence of the early phosphorescence.

Introducing Eqs. (B2), (B4), and (B5) into Eq. (B1), the phosphorescence B_P becomes

$$B_P(t) = \frac{\delta \alpha_1(t) + (\epsilon / \hat{n}_{0\infty}) \alpha_2(t)}{1 + (\delta + 1) / \hat{n}_{0\infty} \alpha_0(t)} D_{2\infty}. \quad (\text{B7})$$

The $\alpha_1(t)$ and $\alpha_2(t)$ decrease as the traps empty. The $\alpha_0(t)$ decrease expresses the effect of a given amount of detrapping producing less emission as the Eu^{*2} concentration n_0 decreases. Recalling that $D_{2\infty} = E_{\infty}$ and using Eq. (A6), one obtains

$$\frac{B_P(t)}{G} = \frac{f'_{\text{ionize}}}{1 + \hat{n}_{0\infty}} \frac{\delta \alpha_1(t) + (\epsilon / \hat{n}_{0\infty}) \alpha_2(t)}{1 + (\delta + 1) / \hat{n}_{0\infty} \alpha_0(t)}. \quad (\text{B8})$$

Equation (B8) was quoted in the text as Eq. (9).

¹C. W. Struck and W. H. Fonger, in *Extended Abstracts, the Electrochemical Society, Spring Meeting, Los Angeles, California, May 10-15, 1970* (The Electrochemical Society, New York, 1970), p. 119; W. H. Fonger and C. W. Struck, *J. Electrochem. Soc.* **118**, 273 (1971).

²H. Forest, A. Cocco, and H. Hersh, *Electrochemical Society, Boston Meeting, RNP 300, 1968* (unpublished).

³H. Forest, A. Cocco, and H. Hersh, *J. Luminescence* **3**, 25 (1970).

⁴C. W. Struck and W. H. Fonger, *J. Luminescence* **1/2**, 456 (1970).

⁵W. H. Fonger and C. W. Struck, *J. Chem. Phys.* **52**, 6364 (1970).

⁶Sublinear, in this paper, means varying as G^α with $\alpha < 1$. Similarly, superlinear means varying as G^α with $\alpha > 1$. In both cases α need not be constant.

⁷R. N. Hall, *Phys. Rev.* **87**, 387 (1952).

⁸W. Shockley and W. T. Read, *Phys. Rev.* **87**, 835 (1952).

⁹K. A. Wickersheim, R. A. Buchanan, and E. C. Yates, in *Proceedings of the Seventh Rare-Earth Research Conference, Coronado, Calif., 1968*, p. 835 (unpublished).

Annihilation of Positrons in Methane*

J. D. McNutt, D. A. Johnson,[†] and V. B. Summerour

Department of Physics, The University of Texas, Arlington, Texas 76010

(Received 8 February 1971)

Positron lifetime spectra have been measured in methane gas at 23 °C over a density range of 5.0×10^{-4} to 1.5×10^{-2} g/cm³. Statistical analysis of the data yields a Z_{eff} of 0.442 ± 0.019 for orthopositronium and a Z_{eff} of 153.3 ± 0.6 for positrons which do not form positronium. Several annihilation mechanisms are discussed in connection with the data.

INTRODUCTION

The annihilation of positrons has been investiga-

ted in many different monatomic and simple diatomic gases, and considerable progress has been made in the theoretical interpretation of the ob-